Flexural Behavior of an Ultrahigh-Performance Concrete I-Girder

Benjamin A. Graybeal, Ph.D., P.E., M.ASCE[1]

Abstract: The flexural behavior of an ultrahigh-performance concrete (UHPC) was investigated through the testing and related analysis of a full-scale prestressed I-girder. A 28 ksi (193 MPa) compressive strength steel fiber reinforced concrete was used to fabricate an 80 ft (24.4 m) long AASHTO Type II girder containing 26 prestressing strands and no mild steel reinforcement. Intermediate and final behaviors, including cracking, flexural stiffness, and moment capacity, were investigated. Test results are compared to predictions based on standard analytical procedures. A relationship between tensile strain and crack spacing is developed. The uniaxial stress-strain response of UHPC when subjected to flexural stresses in an I-girder is determined and is verified to be representative of both the stress and flexural stiffness behaviors of the girder. A flexural design philosophy for this type of girder is proposed.

DOI: 10.1061/(ASCE)1084-0702(2008)13:6(602)

CE Database subject headings: Concrete structures; Concrete beams; Prestressed concrete; Flexural strength; High-strength concrete; Fibers; Girders.

Introduction

Ultrahigh-performance concrete (UHPC) is a new class of concrete that has been developed in recent years. When compared with high performance concrete (HPC), UHPC exhibits superior compressive and tensile mechanical behaviors, as well as exceptional durability properties. A research program was initiated to characterize many of the behaviors relevant to the use of UHPC in the highway bridge industry (Graybeal 2006a,b). Full-scale AASHTO Type II prestressed concrete girders were tested under flexural and shear loadings. The results of the flexural testing program are discussed herein.

The term UHPC covers a broad range of cementitious composite materials that exhibit sets of mechanical and durability properties far advanced beyond conventional concretes. The French led a significant portion of the early development of these materials in corporate, national, and academic research laboratories. This background led to the publication of the Association Française de Génie Civil *Interim Recommendations for Ultra High Performance Fiber-Reinforced Concretes* (Association Française de Génie Civil 2002). This document states that UHPCs tend to have a compressive strength over 21.7 ksi (150 MPa), internal fiber reinforcement to ensure nonbrittle behavior, and a high cementitious materials content. UHPCs also tend to have very low water-to-cementitious materials ratios, minimal or no coarse aggregates, and an optimized gradation of granular materials.

The UHPC studied in this research program is the only concrete of this type currently commercially available in North America. This high cement, high silica fume content concrete has an extremely low water-cementitious materials ratio (less than 0.20) and requires high-range water-reducing admixtures to achieve the correct rheology. This concrete contains no coarse aggregate and is internally reinforced by 0.5 in. (13 mm) long, 0.008 in. (0.2 mm) diameter straight steel fibers that are included at a volumetric ratio of 2%. Further details on the mix composition can be found in Graybeal (2007).

The material characterization research program associated with the research discussed herein focused on quantifying the mechanical and durability properties of this UHPC. Table 1 provides a listing of many of the properties that were quantified using standardized tests. Of particular interest in the realm of structural concrete, after the application of a steam curing treatment this UHPC has a compressive strength of 28 ksi (193 MPa), a tensile cracking strength of 1.3 ksi (9 MPa), and a creep coefficient of 0.29.

The use of this new class of concrete in structural applications has been limited. One reason for the slow implementation is the perceived complexity of the structural behaviors of UHPC components as compared to conventional concrete components as well as the lack of full-scale UHPC component test results. Given the increased material cost of UHPC as compared to conventional concrete, practical use of UHPC structural components will likely require optimization of the component to make use of the advanced mechanical and durability properties. Of primary interest, this optimization frequently leads to the use of the tensile properties of UHPC to carry a portion of the loads imparted on the component. Without an understanding of the UHPC tensile properties as exhibited on the structural component level, the optimal design of said components is not possible.

UHPC tensile properties are distinct from those of conventional concrete due to the increased tensile cracking capacity of the cementitious composite matrix and the crack-bridging behavior of the fiber reinforcement. In contrast to fiber-reinforced conventional concretes, UHPC can exhibit significant, sustained postcracking tensile capacity prior to crack localization, fiber

[1]Research Structural Engineer, Federal Highway Administration, Turner-Fairbank Highway Research Center, 6300 Georgetown Pike, McLean, VA, 22101. E-mail: benjamin.graybeal@fhwa.dot.gov

Note. Discussion open until April 1, 2009. Separate discussions must be submitted for individual papers. The manuscript for this paper was submitted for review and possible publication on January 7, 2008; approved on March 6, 2008. This paper is part of the ***Journal of Bridge Engineering***, Vol. 13, No. 6, November 1, 2008. ©ASCE, ISSN 1084-0702/2008/6-602–610/$25.00.

Table 1. Mechanical and Durability Properties

Material characteristic	Value
Compressive strength—ASTM C39; 28-day strength	28.0 ksi (193 MPa)
Modulus of elasticity—ASTM C469; 28-day modulus	7,600 ksi (52.4 GPa)
Tensile cracking strength—Combined result from four independent test methods	1.3 ksi (9.0 MPa)
Long-term creep (C_{cu})—ASTM C512; 11.2 ksi (77 MPa) sustained load	0.29
Total unrestrained shrinkage—From casting via vibrating wire gauge embedded in ASTM C157 concrete prism	850 microstrain
Coefficient of thermal expansion—AASHTO TP60-00	$8.7\times10^{-6}/°F$ ($15.6\times10^{-6}/°C$)
Chloride ion penetrability—ASTM C1202; 28-day test	18 C
Chloride ion permeability—AASHTO T259; 0.5 in. (12.7 mm) depth	0.004 lb/ft^3 (<0.06 kg/m^3)
Scaling resistance—ASTM C672	No scaling
Abrasion resistance (grams lost)—ASTM C944 2× weight; ground surface	0.0004 lb. (0.17 g) lost
Freeze-thaw resistance (RDM)—ASTM C666A; 600 cycles	96%
Alkali-silica reaction—ASTM C1260; tested for 28 days	Innocuous

pullout, and loss of tensile capacity. Fig. 1 shows a schematic of the three distinct tensile behaviors that UHPC can exhibit: (1) linear-elastic behavior before cracking; (2) postcracking strain hardening behavior and dispersed discrete cracking; and (3) softening behavior during strain localization across specific cracks (Habel et al. 2006). Behavior through the conclusion of strain hardening involves the development of distinct cracks that are closely spaced (less than half of the fiber length) and have small widths (generally measured in tens of micrometers). This portion of the tensile behavior of UHPC is of interest in the design of structural components; softening behavior is of little practical interest as crack localization and fiber pullout coincide with loss of tensile capacity and component failure unless secondary load paths are available.

The research effort discussed herein focused on determining the specific tensile behaviors that this UHPC exhibits when subjected to flexure in a full-scale prestressed AASHTO bridge girder. Of particular interest are the shapes of Parts I and II of the curve shown in Fig. 1, the spacing of the dispersed discrete cracks at various strain levels, the flexural stiffness that a UHPC I-girder displays, and the development of a design philosophy that accounts for the tensile behaviors of UHPC.

It is recognized that the girder cross-sectional geometry tested herein is not necessarily a structurally efficient form for use with UHPC. However, the AASHTO cross section provides a true indication of full-scale structural behaviors of this concrete. Knowledge of these behaviors is necessary for subsequent structural optimizations.

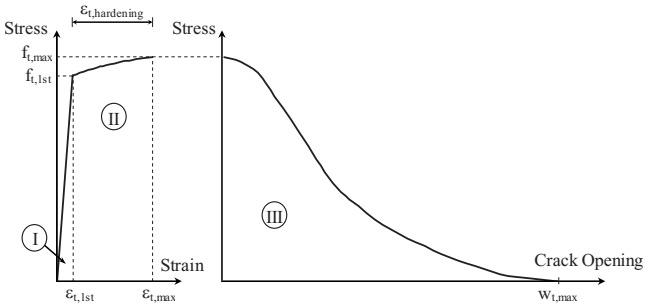

Fig. 1. Tensile behavior of UHPC (Habel et al. 2006, with permission)

Experimental Program

Test Specimen

The test specimen for this research effort was an AASHTO Type II prestressed I-girder. This 36 in. (0.91 m) deep girder was 80 ft (24.4 m) long and contained 26 0.5 in. (12.7 mm) diameter, 270 ksi (1,860 MPa) low relaxation prestressing strands as indicated in Fig. 2. The girder design was modified in three specific ways for this research program. First, the conventional concrete was replaced with UHPC. Second, the girder contained no mild steel reinforcement. Third, the strands in the girder were only jacked to 55% of their ultimate strength due to concern over potential detrimental end region behaviors resulting from the large amount of prestress on this relatively small cross section.

The compressive properties of the UHPC were measured both through the testing of cylinders cast and cured alongside the beam and through the testing of cylinders produced as part of the related material characterization study (Graybeal 2006a). The release of strands was specified to occur when the compressive strength of the UHPC was above 10 ksi (69 MPa). Recognizing the rapid strength gain this UHPC exhibits as it strengthens toward 15 ksi (103 MPa) and the different curing conditions that are present within the girder as compared to within a cylinder, it is assumed that the compressive strength of the girder was 12 ksi (83 MPa) at strand release. The compressive strength of the UHPC girder at the time of flexure testing was 28 ksi (193 MPa) based on cylinder tests, and the modulus of elasticity was 8,100 ksi (55.8 GPa) based on the elastic flexural behavior of the girder. Time-dependent prestressing losses began at stressing and continued for the life of the girder. As such, the compressive strength and modulus of elasticity expressed during prestressing losses vary. Based on the strength to modulus of elasticity relationship presented in Graybeal (2007), a modulus of elasticity of 5,000 ksi (34.5 GPa) was assumed to be representative of the concrete stiffness at strand release and 6,000 ksi (41.4 GPa) was assumed to be representative of the concrete stiffness during prestress losses.

Experimental Investigation

The 80 ft (24.4 m) long girder was tested in flexure on a 78.5 ft (23.9 m) span. The girder was loaded in four point bending, with the point loads each located 3 ft (0.91 m) from midspan as is

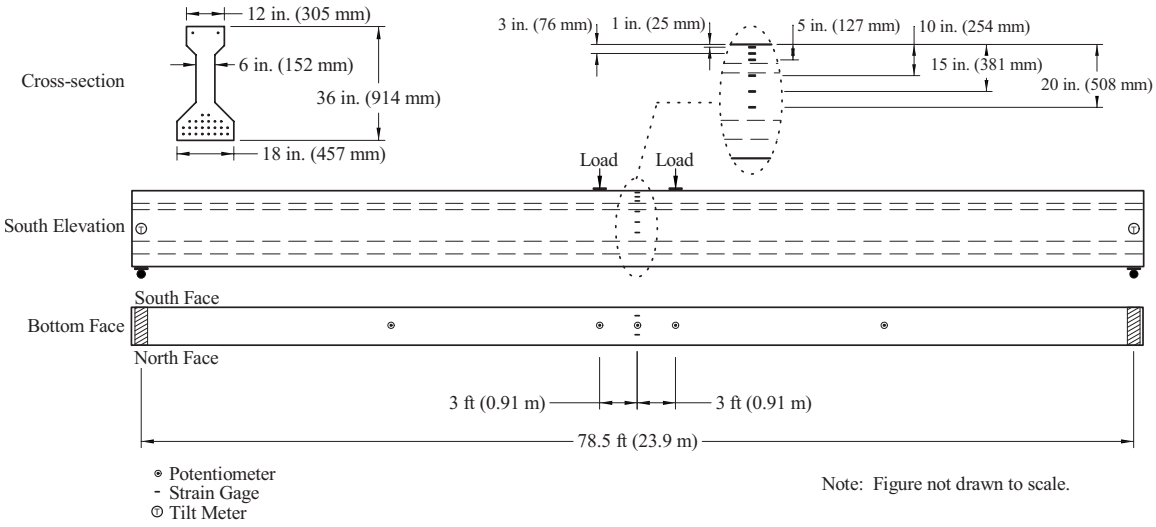

Fig. 2. Cross section, loading configuration, and instrumentation plan

shown in Fig. 2. The girder was instrumented with load cells, with 2 in. (51 mm) gauge length surface-bonded electrical resistance strain gauges, with potentiometers, and with tilt meters. The majority of strain gauges were placed on the midspan cross section in order to capture the strain profile and the neutral axis location throughout the test. Midspan strain gauges were located on the top extreme fiber, bottom extreme fiber, and at 1, 3, 5, 10, 15, and 20 in. (25, 76, 127, 254, 381, and 508 mm) down from the top extreme fiber. The potentiometers measured vertical deflection at midspan, at each load point, and at each quarter point. One tilt meter measured the rotation of the mid-depth of the girder at each bearing location.

The girder was initially loaded in 4 kip (17.8 kN) load steps. After the girder began to sustain inelastic damage and exhibit reduced flexural stiffness, the test was incremented on midspan deflections of 0.2 in. (5 mm) and then 0.5 in. (12.7 mm) until failure. Periodically throughout the test the load level was decreased to approximately 75% of the maximum load previously achieved. The load was then increased and the residual stiffness of the girder was measured. The loading of the girder continued until failure, which was defined as pullout of fiber reinforcement crossing a dominant crack and the subsequent rupturing of the prestressing strands.

Fig. 3 shows the midspan load-deflection response of the girder from initial load application through the peak load of 178 kips (790 kN) occurring at a deflection of 18.5 in. (0.47 m). The load-deflection response shows that the girder behavior began to soften at 75 kips (330 kN) of applied load and a deflection of approximately 3 in. (76 mm). The girder exhibited significant additional load-carrying capacity after initial cracking, due in part to the fiber reinforcement.

The 16 strain gauges located at midspan were used to create a strain profile over the depth of the girder and to identify the location of the neutral axis. Individual gauges were used until their readings became unreliable due to cracking of the underlying concrete. The data from both sides of the girder correlated well. Fig. 4 shows the recorded midspan top flange strain, along with the interpolated neutral axis depth values and extrapolated bottom flange strain values. The figure shows that the neutral axis began to rise at an applied moment of approximately 1,415 k ft (1,920 kN m), corresponding to a load of approximately 78 kips (350 kN). Also note the stability of the neutral axis depth during the unloading and reloading sequences.

Significant audible cracking—which started when the load reached 73 kips (325 kN) and continued throughout the remainder of the test—emanated from the girder. However, these cracking sounds could not be individually correlated to cracks on the surface of the girder. In fact, at loads below approximately 160 kips (700 kN) the cracks were not visible with the naked eye.

The test was halted overnight just after a peak load of 140 kips (620 kN) and a deflection of 12 in. (0.30 m) was reached. Neither inspection of the girder nor the instrumentation results showed that any appreciable changes occurred overnight. Prior to resuming the test the cracks on the bottom of the bottom flange were mapped. Fig. 5 shows photographic results of this mapping at six points along the length of the girder. The crack spacing near midspan was approximately 0.2 in. (5 mm). This spacing had increased to 0.4 in. (10 mm) at 10 ft (3 m) from midspan, 1 in. (25 mm) at 16 ft (4.9 m), and 5 in. (127 mm) at 22 ft (6.7 m).

The peak applied moment prior to failure was 3,225 k ft (4,370 kN m), corresponding to a combined applied plus self-weight moment of 3,540 k ft (4,800 kN m). After the deflection increment bringing the applied load to 178 kips (790 kN) was reached, the midspan deflection continued to increase as the hy-

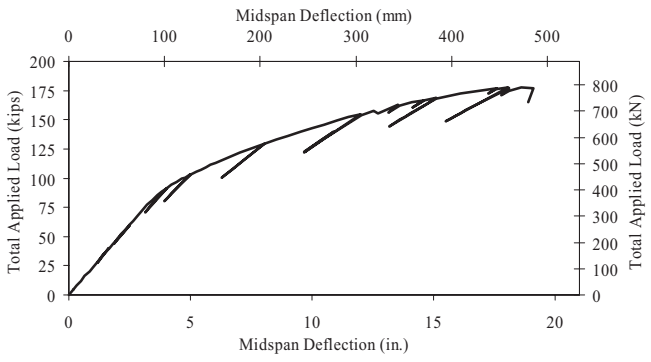

Fig. 3. Flexural behavior of AASHTO Type II UHPC girder

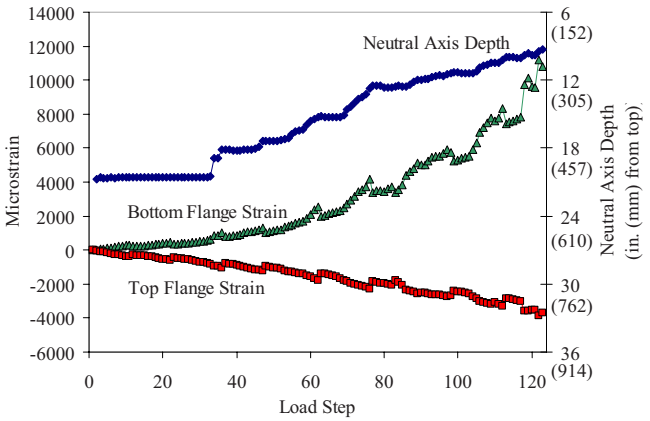

Fig. 4. Strain profile results for midspan of girder

draulically actuated load decreased slightly. After this load step was reached and just prior to failure, a single large crack was observed in the bottom flange and web below the west load point. Unlike any other cracks in the girder, this crack was of sufficient width to be clearly visible to observers from a distance of 16 ft (5 m) and was indicative of fiber pullout occurring at this location. The fiber pullout caused a local stress increase in the strands and precipitated strand rupture, with the girder separating into two unconnected pieces.

Analysis of Test Results

Predictions of Girder Flexural Capacity

The initial, elastic behavior of the girder was analyzed through a strain compatibility analysis. This analysis provided the state of stress in the girder at the initiation of live load application and thus is the starting point for all subsequent flexural analyses. The time-dependent stress losses in the strands resulting from concrete creep, concrete shrinkage, and strand relaxation were approximated to total 14%. This loss value is based on specific material behaviors observed in the associated study of this UHPC (Graybeal 2006a) and its derivation is presented in detail elsewhere (Graybeal 2006b). Thus the overall effective prestressing force was 455 kips (2,020 kN) at an eccentricity of 9.2 in. (0.23 m) below the elastic neutral axis.

A rectangular stress block approximation for the compressive behavior of concrete in flexure allows for a simplified means to predict the flexural behavior of prestressed concrete girders. This empirical relationship has been found to accurately approximate the nonlinear stress-strain behavior of conventional concrete and is thus widely used in flexural provisions of reinforced concrete design specifications. However, two of the assumptions inherent in United States design codes (AASHTO 2007; ACI 2005) that use this analytical technique are violated by the behaviors of this UHPC. First, this UHPC exhibits a compressive stress-strain response that is nearly linear to high stress levels and more closely resembles a triangular stress distribution than the familiar parabolic distribution of conventional concrete (Graybeal 2007). Although this behavior could be accounted for through a modification of the parameters of the rectangular stress block, these design codes currently do not contain provisions allowing the proper modifications to occur. Second, this UHPC exhibits a sustained tensile capacity after cracking to high tensile strain levels (Graybeal 2006b). Code-based ultimate flexural capacity calculations assume that the concrete carries no tensile force, thus these calculations may be significantly in error if applied to UHPC. For both of these reasons, the use of the rectangular stress block approximation and associated analytical methods to predict the behavior of UHPC girders may not be warranted.

To illustrate this fact, the following presents an analysis of the UHPC girder based on the standard code-based analytical method. This result is compared to the experimentally determined flexural capacity of the UHPC girder and to the capacity that this code-based method would predict for a conventional HPC prestressed girder. Recall that the peak load applied to the girder was 178 kips (790 kN), corresponding to an applied moment of 3,225 k ft (4,370 kN m).

A girder geometrically equivalent to that tested in this study was analyzed assuming $f'_c=8$ ksi (55 MPa), $\alpha=0.85$, and $\beta_1=0.65$. These calculations resulted in a calculated flexural capacity of 1,700 k ft (2,300 kN m), a neutral axis depth of 16.4 in., and a bottom fiber tensile strain at failure of 0.0036. Given that the rectangular stress block model is widely accepted as being representative of the compressive flexural behavior of conven-

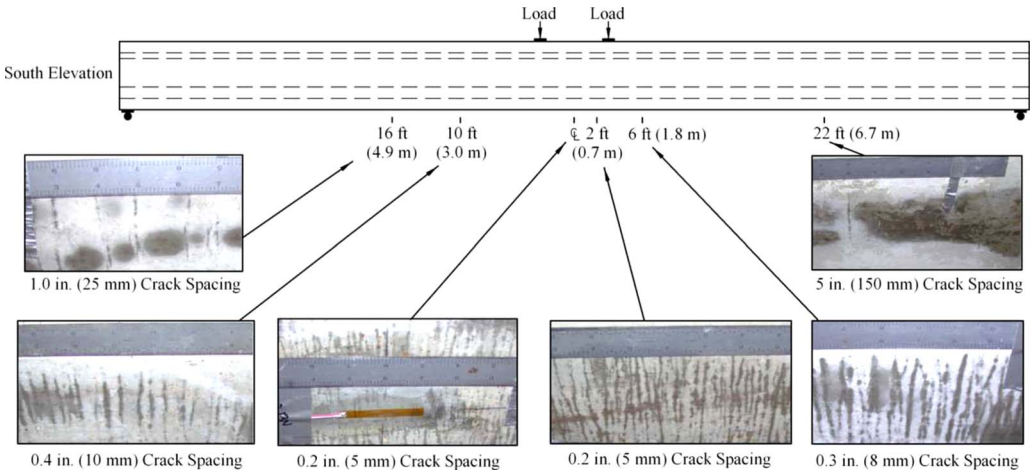

Fig. 5. Crack spacing on bottom flange of girder after 12 in. (305 mm) of midspan deflection

tional and high-performance concretes, this calculation demonstrates that UHPC I-girders can display significantly increased flexural capacity as compared to similar HPC girders.

The analysis was then completed again with two more sets of parameters: (1) f'_c=28 ksi (193 MPa), α=0.85, β_1=0.65; and (2) f'_c=28 ksi (193 MPa), α=0.75, β_1=0.667. The first of these is equivalent to the analysis above with only the compressive strength being modified. The second allows the rectangular stress block to mimic the compressive behavior of a concrete that behaves linear elastically through failure. In both cases the calculated flexural capacity is approximately 73% of the observed capacity. However, to reach this capacity both of these calculations predict that the extreme tensile fiber strain would be greater than 0.016 and the neutral axis depth would be approximately 5 in. (130 mm) below the top of the girder. This strain is well beyond the experimentally observed strain at which the fiber reinforcement pulled out and the prestressing strands ruptured in the physical girder test. This neutral axis is also much higher than was observed in the laboratory test just prior to girder failure. In total, these results indicate that common design code-based calculation methods do not provide an accurate representation of the flexural behaviors observed.

Finally, a direct comparison of the flexural capacity results was completed between the girder tested in this study and a girder tested by Russell and Burns (1993). Russell and Burns tested a 46 in. (1.17 m) deep decked I-girder. This girder had a 6 ksi (41 MPa), 72 in. (1.83 m) wide top flange, and was prestressed with 28 0.5 in. (12.7 mm) strands. This 28% deeper girder displayed a similar moment capacity to the UHPC girder tested in the present study. Achieving a similar flexural capacity with a significantly shallower girder demonstrates just one of the potential applications for which UHPCs may find use.

Cracking Behavior of UHPC

The tensile cracking behavior of this prestressed UHPC girder was observed to be significantly different than would be expected in a conventional concrete girder. As shown in Fig. 5, the extreme tensile fiber of this prestressed girder displayed a very high crack density. Recall that the crack spacing observations were recorded when the total applied load on the girder was 140 kips (620 kN). The crack spacing at any cross section along the span was observed to be inversely proportional to the maximum tensile strain experienced by the bottom fiber as a result of flexural forces applied to the girder. Thus, the load and strain data collected during the testing of the girder, along with the crack spacing density observations, allow for the derivation of a relationship between the curvature-based UHPC extreme tensile fiber strain and the observed crack spacing on the extreme tensile fiber of the prestressed girder. This relationship could prove useful for two reasons. First, crack spacing could provide an indication of maximum tensile strain experienced by a UHPC structural component whose load history is unknown. Second, the crack spacing could provide an indication of whether a UHPC laboratory component exhibited the expected tightly spaced tensile cracking behavior necessary for significant postcracking tensile capacity.

The basic assumption required to initiate the derivation of this relationship is that the girder is undergoing pure flexural behavior with plane sections remaining plane. Under pure flexural behavior, the observed neutral axis location and curvature of the midspan cross section can be used to calculate the midspan effective strain in the extreme tensile fiber of the girder at any applied moment. These calculated strains in the extreme tensile fiber at midspan of the test girder are presented in Fig. 4. At the load step where crack spacing observations were recorded the extreme tensile fiber strains along the length of the girder were then determined. The prestress forces, the girder self-weight, and the applied loads are accounted for within these calculations.

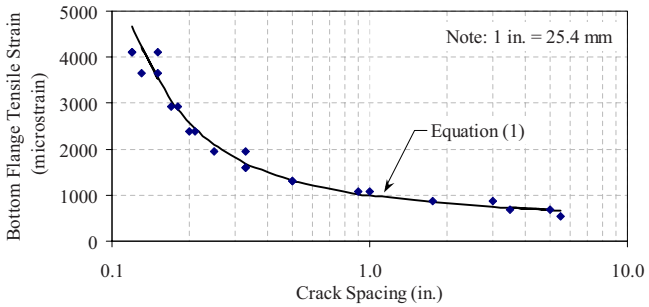

Fig. 6. Tensile strain related to flexural crack spacing

The crack spacing versus strain results are presented in Fig. 6. This figure, presented in semilog format, also shows a curve representing the best-fit equation for the results. Eq. (1) defines this curve with the strain, ε, in microstrain calculated from the crack spacing, s_{cr}, in inches or millimeters. This equation has an R-squared value of 0.952

$$\varepsilon = 450 + \frac{500}{\sqrt{s_{\text{cr}}}} + \frac{40}{s_{\text{cr}}^2} \quad \text{with } s_{\text{cr}} \text{ in inches}$$

$$\varepsilon = 450 + \frac{2{,}520}{\sqrt{s_{\text{cr}}}} + \frac{25{,}800}{s_{\text{cr}}^2} \quad \text{with } s_{\text{cr}} \text{ in millimeters} \qquad (1)$$

Tensile Stress-Strain Behavior of UHPC

The effective structural use of UHPC requires knowledge of its uniaxial stress-strain behavior. An analytical derivation of the uniaxial stress-strain response of the UHPC was obtained from the experimental results of the flexural testing of this girder. One principal component of this derivation was the strain profile on the midspan cross section of the girder. Another important experimental result was the moment applied to the midspan of the girder throughout the test. Finally, both an approximation of the compressive stress-strain response of UHPC and an approximation of the tensile stress-strain response of 270 ksi low relaxation prestressing strand were necessary and were referenced from Graybeal (2007) and Caltrans (2006), respectively.

Results from the previously discussed strain compatibility analysis were used here again to define the state of strain and stress in the girder prior to the initiation of flexural testing. From this analysis, the compressive stresses in the concrete at the initiation of the flexure test were calculated to be 1.0 ksi (6.9 MPa) at the top of the midspan cross section and 1.5 ksi (10.3 MPa) at the bottom of the midspan cross section. The calculated stresses in the strands ranged from 122 ksi (843 MPa) in the top flange strands to 119 ksi (820 MPa) in the lowest bottom flange strands.

These results provide the basis for the moment-curvature analysis that was completed to determine the full uniaxial stress-strain behavior of UHPC in this prestressed I-girder. In contrast to a standard moment-curvature analysis wherein known concrete and steel stress-strain behaviors are applied to a cross section whose curvature is adjusted until internal and external moments

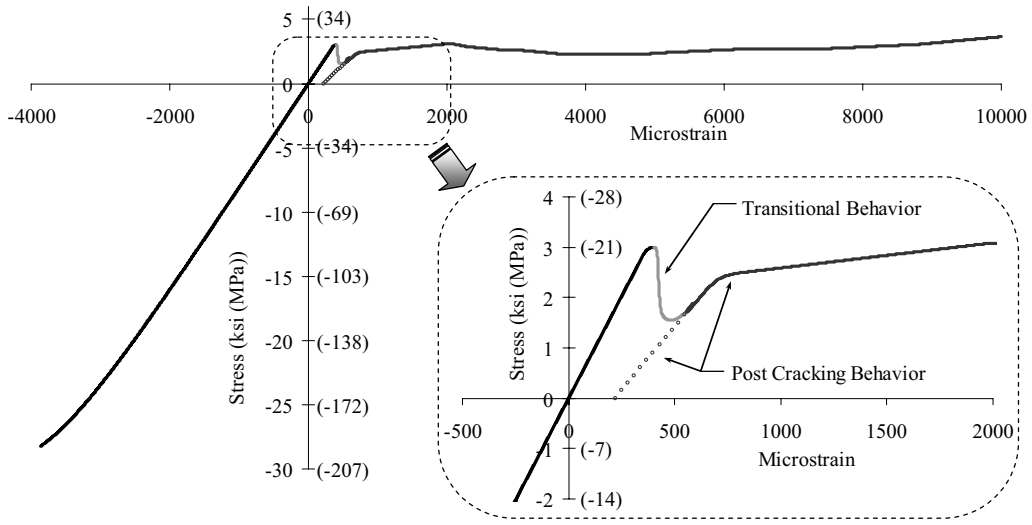

Fig. 7. Analytically derived uniaxial stress-strain behavior of UHPC in prestressed I-girder

reach equilibrium, in this analysis the tensile portion of the concrete stress-strain response is the unknown variable.

The midspan cross section was discretized into 72 concrete slices and five prestressing strand slices parallel to the neutral axis. The measured strain values from the strain gauges on the midspan cross section were used to define the state of strain in each slice over the depth of the midspan cross section at each load step. The tensile portion of the uniaxial stress-strain response for the UHPC was then assumed and the forces on the cross section at each load step were determined. The summation of the forces in the concrete and the strands were compared with one another to ensure that the internal forces on the cross section were in equilibrium at each load step. After many trial UHPC tensile stress-strain responses, the response shown in Fig. 7 was selected as being acceptably representative of the UHPC's behavior throughout the loading history. On all loading steps, the absolute values of the concrete and strand forces are within 7% of one another.

Fig. 7 can be considered to be composed of four separate curves, each defining a portion of the behavior. In compression, the relationship defined elsewhere for UHPC compressive behavior (Graybeal 2007) is used, with a compressive strength of 28 ksi (193 MPa) and a modulus of elasticity of 8,100 ksi (55.8 GPa). The initial tensile behavior of UHPC is considered to be linear elastic with an 8,100 ksi (55.8 GPa) modulus of elasticity; thus it is coincident with the initial slope of the compression behavior. The postcracking behavior curve for UHPC is indicated in Fig. 7 with an initial modulus of elasticity of 5,000 ksi (34.5 GPa). The intermediate portion of the behavior is the tensile transition zone during the initial cracking of the concrete. This transition allows the UHPC to transform from an uncracked, elastic material into a significantly cracked material that is still capable of carrying tensile loads.

Note that according to this model the UHPC carries 3.0 ksi (20.7 MPa) of tensile stress before the cross section becomes sufficiently cracked to cause a change in the slope of the tensile stress-strain response. This value is well above the UHPC tensile cracking strength values ranging from 1.0 to 1.5 ksi (7–10 MPa) that have been experimentally determined elsewhere (Chanvillard and Rigaud 2003; Rossi 1997; Li and Lepech 2004; Graybeal 2006a). Other studies within this research program have shown that tensile behaviors in small-scale specimens without discrete reinforcement tend to occur with less crack density and larger crack widths as compared to full-scale prestressed structural components. The behavior of small-scale tension specimens is more indicative of lower bound tensile behaviors than of the behaviors that could be expected if secondary tensile load paths (i.e., strands or mild steel reinforcement) were present as is the case in the tension flange of a prestressed girder. Tension stiffening as exhibited by fiber reinforced concretes also contributes to the girder's increased tensile capacity (Abrishami and Mitchell 1997; Bischoff 2003; Chao et al. 2007).

To complete this analysis, the unloading and reloading behaviors of UHPC were considered. After UHPC undergoes inelastic deformation, subsequent unloading and reloading of the concrete is modeled as linear elastic behavior with a reduced effective modulus of elasticity. This behavior continues until the previous maximum strain in the load history is exceeded. In this analysis, UHPC not subjected to peak tensile or compressive strains was assumed to behave linear elastically with a stiffness equal to the secant modulus of elasticity of the largest strain ever attained. This model was used in both tension and compression. For the postcracking tensile behaviors, the origin for the secant modulus was shifted to the location where the dotted curve intersects the abscissa in Fig. 7. This location was chosen based on the moment-curvature analysis and is consistent with the fact that cracking (and the resulting load transfer, partial fiber debonding, and fiber bending) necessarily causes an irrecoverable displacement to occur across a crack. In the tensile cracking transition region, the secant moduli were calculated just before and after the transition region. The secant values in the transition region were then linearly interpolated from these bounding values.

A comparison of the analytical and experimental results is shown in Fig. 8. The derived internal forces on the cross section were used to determine the internal moment on the girder midspan at each load step. The load cell readings captured throughout the loading history were used to determine the external moments on the midspan cross section. The experimental and analytical results compare well until the final load steps of the test. Toward the end of the loading history the model tends to overestimate the internal moment, which is explainable by two reasons. First, given that only the strain gauges bonded to uncracked concrete provided reliable results, the experimentally determined strain profile on the cross section became less accurate at high loads when the cross section was significantly cracked and the neutral

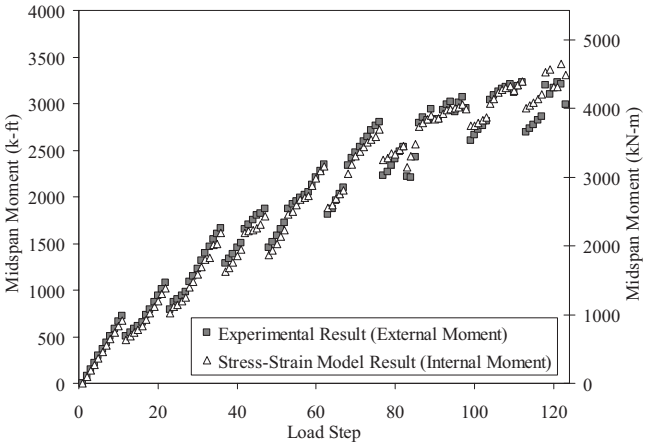

Fig. 8. External and internal moments on midspan cross section

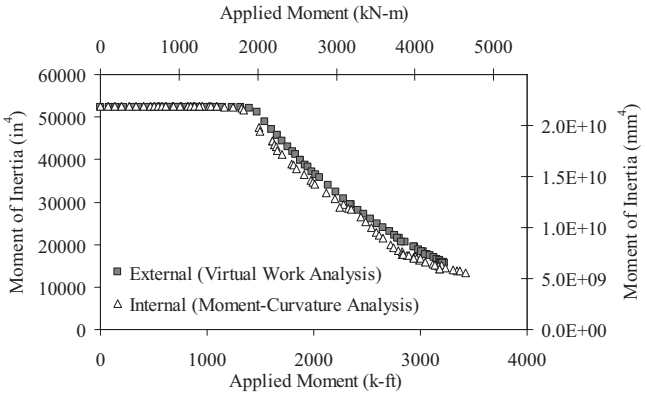

Fig. 9. Externally and internally determined effective moment of inertia

axis had moved closer to the top flange. Second, the analytical method used to determine the uniaxial stress-strain response was more robust at lower strains as this portion of the stress-strain response was utilized during the calculations performed at every load step, while higher strain portions of the response were only engaged at higher applied load levels. Therefore, greater certainty is built into the lower tensile and compressive strain ranges than can be expected in the higher strain ranges.

Flexural Stiffness

The constitutive model for the stress-strain response of this UHPC was also analyzed in terms of the flexural stiffness of the girder. Although a UHPC cross section is generally modeled as carrying tensile forces across tensile cracks, in reality only the internal steel fiber reinforcement that comprises a small fraction of the volume of the UHPC carries any significant tensile forces across cracks. Additionally, as discussed earlier, the flexural tensile cracks in UHPC tend to be of very small width and very closely spaced. As such, the postcracking tensile flexural behavior of UHPC is actually comprised of elastic straining of uncracked concrete, elastic straining of steel fibers bridging cracks, and to a lesser extent plastic bending of nonperpendicular fibers bridging cracks and partial debonding of fibers at their interface with the UHPC matrix. The occurrence of these primarily elastic behaviors throughout a flexural member, even after cracking, necessitate that the constitutive stress-strain model be consistent with the deformations observed. As will be demonstrated below, the flexural deformations of this girder can be modeled through a rational, mechanics-based methodology.

The midspan cross-sectional stiffness that results from the uniaxial stress-strain behavior derived previously and presented in Fig. 7 was calculated for each load step. As with normal concrete, UHPC flexural stiffness in compression and in tension prior to cracking can be determined through a straightforward calculation based on the uncracked moment of inertia and the modulus of elasticity of the concrete at the strain level that it is experiencing. After cracking, tensile behavior of UHPC is very different from conventional concrete, with the UHPC carrying stress and exhibiting axial stiffness. The postcracking deformation behaviors of this concrete were modeled through a combination of the uncracked moment of inertia, the uniaxial stress-strain response, and the secant modulus of elasticity at the peak tensile strain level that the UHPC had experienced. The uncracked moment of inertia is used here as this model accounts for cracking of UHPC through a decrease in stress capacity, thereby smearing the concentrated larger forces carried by the fibers, instead of through decreasing the effective area of the cross section and maintaining the higher stress levels that actually occur in the fibers. The resulting flexural stiffness of the girder cross section is plotted as a function of the applied moment in Fig. 9. Note that the plot assumes a constant modulus of elasticity at 8,100 ksi (55.8 GPa).

The check on this result is provided through a comparison with the overall flexural stiffness exhibited by the girder throughout the test. A virtual work analysis was performed to determine the flexural stiffness of any cross section along the length of the girder as a function of the self-weight and applied moment on the girder at that location. In this analytical technique, the moment on the girder is multiplied by the moment generated in the equilibrium system by a "dummy" load at the location where the deflection is desired. Eq. (2) provides the basis for this analysis. The integration, or in this case the summation, of nearly 1,000 discrete cross-sectional slices along the length of the girder provides the solution. Note that shear deformations were excluded from the analysis as preliminary calculations demonstrated that they were of minimal consequence

$$\text{Deflection} = \int_0^{\text{Length}} m(x)\frac{M(x)}{EI(x)}dx \tag{2}$$

In this analysis the UHPC modulus of elasticity was held constant and the moment of inertia was allowed to vary, with their product defining the overall flexural stiffness along the length of the girder, $EI(x)$.

The full pre- and postcracking behavior of the girder was then determined. First, a potential flexural stiffness, EI, was proposed for each self-weight plus applied load moment, M, on the girder. The virtual work analysis was performed to determine the resulting deflections and rotations at each of the potentiometers and tilt meters throughout the test. The analytical results were then compared with the experimental observations at the potentiometers and tilt meters, and the EI versus M relationship was revised accordingly. The analyses were repeated until a sufficiently accurate flexural stiffness was determined. Fig. 9 graphically presents the relationship between the moment on any cross section of the girder and the girder's observed flexural stiffness at that cross section as determined via this virtual work analysis.

In terms of the flexural stiffness of UHPC, the result generated by the moment-curvature model from the midspan cross section is consistent with the result generated by the virtual work model of

the girder's overall behavior. The internal flexural stiffness result is always within 10% of the external result. The comparability of these results shows that the UHPC flexural stiffness can be addressed directly through knowledge of the constitutive stress-strain relationship.

Flexural Design of UHPC I-Girders

Based on the experimentally observed behaviors and the analytical results, a flexural design philosophy for UHPC I-girders has been developed. The design philosophy detailed herein is similar to portions of some UHPC structural design procedures detailed elsewhere (Association Française de Génie Civil 2002; Casanova and Rossi 1996; Gowripalan and Gilbert 2000; Uchida et al. 2005).

The design of a prestressed UHPC I-girder for flexure requires two things. First, a conservative approximation of the UHPC's uniaxial stress-strain response must be applied to the cross section. Second, the occurrence of the expected flexural behaviors must be ensured. Of primary importance, sufficient prestressing strands or mild steel reinforcement must exist in the primary flexural tensile regions so that cracks in the UHPC exhibit small widths and close spacings. Without sufficient gross reinforcement restraining the tensile flexural regions, individual cracks will begin to widen as the fibers pull out and tightly spaced cracks such as that shown in Fig. 5 will not occur.

Determining a sufficiently conservative approximation of UHPC uniaxial stress-strain behavior depends on the intended structural application and on the prescribed design limits. In a situation where cracking of the girder is not allowed at service loads, the girder can be designed using typical prestressed concrete design procedures with the service loads limited to a percentage of the first-cracking moment of the UHPC. In a situation where a minimal amount of cracking will be allowed at service loads, a postcracking uniform tensile stress capacity will need to be assumed. Finally, for the strength limit states, a full compressive and tensile stress-strain response will be required. This response will include an effective tensile strain that causes fiber pullout, a limiting tensile stress capacity relevant to strains below the fiber pullout strain, and a limiting compressive strength.

Until a significant number of full-scale flexure tests are completed, it will not be possible to present a calibrated set of conservative parameters for use in the flexural design of UHPC prestressed girders. Nonetheless, a suggested uniaxial stress-strain response for UHPC based on the results detailed earlier in this paper could be described as follows. First, the UHPC could be assumed to behave linear elastically in compression up to 0.85 times the compressive strength. This is reasonable since this UHPC has been demonstrated to remain within 5% of linear elastic behavior up to over 90% of its compressive strength (Graybeal 2006a). Second, UHPC subjected to tensile strains below the tensile pullout strain could be assumed to behave in an elastic-perfectly plastic fashion at a conservative percentage of the postcracking tensile capacity. This is reasonable since it allows the designer to utilize some tensile capacity while staying within the envelope defined by experimentally observed tensile stress-strain behaviors. Finally, a limiting tensile strain capacity must be defined as fiber pullout is likely to occur prior to strand rupture and may lead to girder failure.

For the UHPC discussed herein, a uniaxial stress-strain response for use in design could include the following:

1. Compressive strength of 24 ksi (165 MPa) corresponding to 0.85 times the observed steam-treated compressive strength of this concrete;
2. Tensile capacity of 1.5 ksi (10.3 MPa), corresponding to 0.5 times the pre- and postcracking uniaxial tensile capacity derived from the girders response;
3. Modulus of elasticity of 7,600 ksi (52.4 GPa), corresponding to the elastic modulus that this UHPC exhibits as determined via compression tests on cylinders; and
4. Limiting tensile strain of 0.007 corresponding to 70% of the tensile strain observed in the extreme tensile fiber of the girder just prior to gross cracking, strain localization, and girder failure.

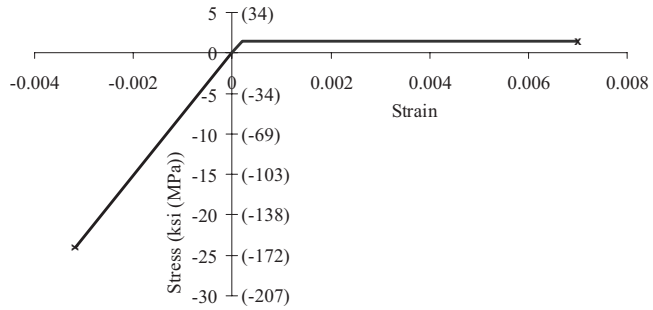

Fig. 10. Simplified uniaxial stress-strain behavior for I-girder flexural design

Fig. 10 graphically presents this simplified stress-strain behavior.

Using this stress-strain response, the predicted ultimate applied moment capacity of the UHPC girder discussed herein is 2,440 k ft (3,310 kN m), 76% of the experimentally determined applied moment capacity. As compared to the conventional methods for analyzing prestressed concrete girders discussed earlier in this paper, the method presented here is admittedly significantly more complex. However, it is also rational in that it conservatively addresses the actual behaviors exhibited by this UHPC I-girder. The fact that this moment capacity of 2,440 k ft (3310 kN m) is only 4% greater than the value calculated via the method presented in United States design codes is of little consequence; the specifications in these design codes do not address the actual behaviors of UHPC and thus would be unlikely to consistently predict capacities corresponding to a particular percentage of the true ultimate capacity.

Conclusions

Based on the results of this investigation, including the experimental testing to flexural failure of a UHPC I-girder, the following conclusions are drawn:

1. UHPC I-girders will display flexural capacities larger than those of conventional concrete girders with similar cross-sectional geometry;
2. The interaction of the fiber reinforcement and the UHPC matrix allows small width, closely spaced cracks to occur and allows the UHPC to carry tensile loads after cracking;
3. The crack spacing in the tension flange of a UHPC I-girder is inversely proportional to the maximum tensile strain observed in said cracked region;
4. A full uniaxial stress-strain response of UHPC subjected to flexural loading in a prestressed I-girder was determined. This rationally determined stress-strain response correlated

well with the girder's experimentally recorded load and deflection behavior; and

5. The flexural design of UHPC I-girders can be completed in a rational manner through the use of a conservative approximation of the stress-strain behavior.

Acknowledgments

The research which is the subject of this paper was funded by the Federal Highway Administration. The writer gratefully acknowledges this support. The publication of this article does not necessarily indicate approval or endorsement of the findings, opinions, conclusions, or recommendations either inferred or specifically expressed herein by the Federal Highway Administration or the United States Government.

Notation

The following symbols are used in this paper:

$EI(x)$ = flexural stiffness of girder at any location x;
f'_c = compressive strength of concrete;
$f_{t,\max}$ = concrete tensile stress at conclusion of strain hardening behavior;
$f_{t,1st}$ = concrete tensile stress at first cracking;
$M(x)$ = moment on girder from self-weight plus applied load at any location x;
$m(x)$ = moment on girder from dummy load application at any location x;
s_{cr} = crack spacing;
$w_{t,\max}$ = concrete crack width at conclusion of fiber pullout;
α = factor applied to f'_c such that equivalent uniformly stressed compression zone has correct resultant force;
β_1 = ratio of depth of equivalent uniformly stressed compression zone to depth of actual compression zone;
ε = strain in concrete;
$\varepsilon_{t,\text{hardening}}$ = total concrete tensile strain between $\varepsilon_{t,1st}$ and $\varepsilon_{t,\max}$;
$\varepsilon_{t,\max}$ = concrete tensile strain at conclusion of strain hardening behavior; and
$\varepsilon_{t,1st}$ = concrete tensile strain at first cracking.

References

AASHTO. (2007). *AASHTO LRFD bridge design specifications*, 4th Ed., Washington, D.C.

Abrishami, H., and Mitchell, D. (1997). "Influence of steel fibers on tension stiffening." *ACI Struct. J.*, 94(6), 769–776.

American Concrete Institute (ACI). (2005). "Building code requirement for structural concrete." *ACI-318–05*, Detroit.

Association Française de Génie Civil. (2002). *Interim recommendations for ultra high performance fibre-reinforced concretes*, Paris, France.

Bischoff, P. (2003). "Tension stiffening and cracking of steel fiber-reinforced concrete." *J. Mater. Civ. Eng.*, 15(2), 174–182.

California Department of Transportation (Caltrans). (2006). "Seismic design criteria." June.

Casanova, P., and Rossi, P. (1996). "Analysis of metallic fibre-reinforced concrete beams submitted to bending." *Mater. Struct.*, 29, 354–361.

Chanvillard, G., and Rigaud, S. (2003). "Complete characterization of tensile properties of Ductal® UHPFRC according to the French recommendations." *Proc., 4th Int. RILEM Workshop on High Performance Fiber Reinforced Cement Composites (HPFRCC4)*, Ann Arbor, Mich., Springer, The Netherlands.

Chao, S., Liao, W., Wongtanakitcharoen, T., and Naaman, A. (2007). "Large scale tensile tests of high performance fiber reinforced cement composites." *Proc., 5th Int. RILEM Workshop on High Performance Fiber Reinforced Cement Composites (HPFRCC5)*, Mainz, Germany.

Gowripalan, N., and Gilbert, R. I. (2000). *Design guidelines for RPC prestressed concrete beams*, VSL (Australia) Pty. Ltd., Sydney, Australia.

Graybeal, B. A. (2006a). "Material property characterization of ultra-high performance concrete." *Rep. No. FHWA-HRT-06-103*, Federal Highway Administration, Washington, D.C.

Graybeal, B. A. (2006b). "Structural behavior of ultra-high performance concrete prestressed I-girders." *Rep. No. FHWA-HRT-06-115*, Federal Highway Administration, Washington, D.C.

Graybeal, B. A. (2007). "Compressive behavior of an ultra-high performance fiber reinforced concrete." *ACI Mater. J.*, 104(2), 146–152.

Habel, K., Denarié, E., and Brühwiler, E. (2006). "Time dependent behavior of elements combining ultra-high performance fiber reinforced concretes, (UHPRFC) and reinforced concrete." *Mater. Struct.*, 39, 557–569.

Li, V., and Lepech, M. (2004). "Crack resistant concrete material for transportation construction." *Proc., Transportation Research Board Conf.*, TRB, Washington, D.C.

Rossi, P. (1997). "High performance multimodal fiber reinforced cement composites (HPMFRCC): The LCPC experience." *ACI Mater. J.*, 94(6), 478–483.

Russell, B. W., and Burns, N. H. (1993). "Static and fatigue behavior of pretensioned composite bridge girders made with high strength concrete." *PCI J.*, 38(3), 116–128.

Uchida, Y., Niwa, J., Tanaka, Y., and Katagiri, M. (2005). "Outlines of 'Recommendations for design and construction of ultra high strength fiber reinforced concrete structures' by JSCE." *Proc., Int. Workshop on High Performance Fiber Reinforced Cementitious Composites in Structural Applications*, Honolulu.